PHYSICAL REVIEW B **80**, 184113 (2009)

Expansion-limited aggregation of nanoclusters in a single-pulse laser-produced plume

E. G. Gamaly,[1,*] N. R. Madsen,[1,†] D. Golberg,[2] and A. V. Rode[1]
[1]*Laser Physics Centre, Research School of Physics and Engineering, The Australian National University, Canberra, Australian Capital Territory 0200, Australia*
[2]*World Premier International Center for Materials Nanoarchitectonics (MANA), National Institute for Materials Science, Tsukuba, Ibaraki 305-0044, Japan*
(Received 23 April 2009; revised manuscript received 15 July 2009; published 19 November 2009)

Formation of carbon nanoclusters in a single-laser-pulse created ablation plume was studied both in vacuum and in a noble gas environment at various pressures. The developed theory provides cluster radius dependence on combination of laser parameters, properties of ablated material, and type and pressure of an ambient gas in agreement with experiments. The experiments were performed on carbon nanoclusters formed by laser ablation of graphite targets with 12 picosecond 532 nm laser pulses at MHz-range repetition rate in a broad range of ambient He, Ar, Kr, and Xe gas pressures from 2×10^{-2} to 1500 Torr. The experimental results confirmed our theoretical prediction that the average size of the nanoparticles depends weakly on the type of the ambient gas used, and is determined exclusively by the single laser pulse parameters even at the repetition rate as high as 28 MHz with the time gap 36 ns between the pulses. The most important finding relates to the fact that in vacuum the cluster size is mainly determined by hydrodynamic expansion of the plume while in the ambient gas it is controlled by atomic diffusion in the gas. We demonstrate that the ultrashort pulses can be used for production of clusters with the size less than the critical value, which separates the particles with properties drastically different from those of a material in a bulk. The presented results of experiments on formation of carbon nanoclusters are in close agreement with the theoretical scaling. The developed theory is applicable for cluster formation from any monatomic material, such as silicon for example.

DOI: 10.1103/PhysRevB.80.184113 PACS number(s): 81.07.−b, 78.67.Bf, 52.38.Mf

I. INTRODUCTION

One of the major problems in nanotechnology resides in the development of efficient methods for controlled formation of nanoclusters with desired size and properties that could be then scaled up to industrial production. The first step in the "bottom-up" formation process is to decompose the initial material into a preferably atomic state via ablation, form a cloud of hot atoms and create temperature and density conditions necessary for assembly of the atoms by "sticky" collisions into different nanostructures. These conditions should be maintained during the period necessary for assembly of a cluster of desirable size. The formation conventionally occurs during the diffusion of a hot atomic cloud through a nonreacting ambient gas that serves as a confinement.

Laser ablation has proven to be an efficient method for producing nanoclusters of different atomic content, shape and internal structure.[1–14] Such techniques have been used for production of nanoclusters since the early eighties. Initially long pulse (10–30 ns), low repetition rate (10–30 Hz), commercially available excimer and Q-switched Nd:YAG lasers with average intensity per pulse of $(2-4)\times10^9$ W/cm^2 on the target surface, were employed. Metal and metal oxide clusters,[5–7] fullerenes,[8,9] carbon and boron nitride nanotubes,[1,3,4,9,10] silicon clusters,[12–14] and many other structures have been produced with laser ablation in similar conditions. Special conditions are often required to promote a particular type of structure to grow. For example, in the case of carbon nanotube growth in a low-repetition rate regime, the laser plume cools down after the pulse below the minimal temperature required for the nanotube formation due to the long gap between the successive pulses. Therefore, additional heating of the ambient gas is necessary in order to maintain the proper conditions for nanotube growth. Large nanoclusters such as nanotube growth by low-repetition rate ns-pulse lasers conventionally form during the laser plume interaction with an ambient gas in a chamber placed into a furnace with controlled temperature and under a continuous flow of a noble gas.

The advent of femtosecond lasers with repletion rates up to 100 MHz and higher, along with a better understanding of the physics of ultrafast laser-matter interaction and cluster formation process, allowed the implementation of an approach to the formation of nanoclusters by single ultrashort laser pulses. It has been shown possible to control the cluster size by choosing the optimum combination of laser-target parameters, eliminating additional heating and even removing the necessity for ambient gas in the chamber.[15] It should be emphasized that ablation by long and short laser pulses occurs in very different laser-matter interaction conditions. In order to ablate the same amount of material with a short pulse, one should apply much higher laser intensity approximately in inverse proportion to the pulse duration. For example, laser ablation with a 100 fs pulse requires the intensity to be above 10^{13} W/cm^2,[16–19] while with 10 ns pulses, the same material is ablated at much lower intensities $\sim10^8-10^9$ W/cm^2.[16] The depth of the material ablated per single short laser pulse is of the order of the skin-depth $l_s=\lambda/2\pi k$, which is typically of the order of 20–50 nm per pulse; here λ in the laser wavelength and k is the imaginary part of the complex refractive index. Alternatively, in the case of long pulse ablation, the characteristic ablation depth is of the order of the heat conduction depth per pulse $\sim(at_p)^{1/2}$, which is generally about a micron per pulse; here

a is the thermal diffusivity in $[\mathrm{cm}^2/\mathrm{s}]$ of the target material and t_p is the pulse duration.[17,18] Correspondingly, the number of atoms evaporated per pulse differs by orders of magnitude.

The size of a cluster has a significant effect upon various material properties and, therefore, provides a relatively simple experimental avenue to control those properties. There is a critical cluster size of a few nanometers that separates atomic ensembles composed of the same atoms but possessing the different material properties when compared to the bulk properties. Melting and boiling points, conductivity, electronic structure etc. in a cluster with a size smaller than the critical size are drastically different from those of the same material in bulk. It appears that nanoclusters below the critical size and smaller can be produced by a single ultrashort laser pulse both in vacuum and in ambient gas. In this work we are, therefore, attempting to control the properties of carbon nanoclusters, which are the building blocks for nanomaterial, via control over their size.

When the laser intensity is close to the ablation threshold it is possible to produce an uncontrollable plume, which contains the mixture of liquid droplets, flakes, and wide range of different macroscopic and microscopic particles.[20] Direct removal of dimers or multiatomic clusters is energetically unfavorable and kinetically improbable from the physical viewpoint. Indeed, one needs to supply simultaneously to at least two bounded atoms the energy in excess of their binding energy with the surrounding solid at the same time keeping their mutual bonding (with twice less energy) intact. This only can happen randomly when a specific arrangement of material defects in some place of the target occurs. We are using high intensity well above the ablation threshold, producing the atomized plume in our experiments. Total atomization in the plume was proved in a number of works on fs-laser ablation and deposition of high surface quality diamond-like films, where the laser intensity was several times above the ablation threshold—see, for example, S. Amoruso *et al.*[21] Carbon atoms re-ensemble into clusters in an expanding plume in a process that controlled by the density and temperature in the plume directly steered by the laser parameters.

The reasoning behind our approach is as follows. The temperature and density of atoms in the adiabatically expanding plume remain appropriate for formation of clusters through the atom-to-atom and atom-to-cluster attachments over a certain time period after the laser pulse. The longer this period of high density and temperature the more successive inelastic collisions occur in the plume, and hence, the larger the cluster may form. Thus, the plume expansion time in vacuum is a major factor in determining the cluster size. This time depends on the combination of laser and material parameters. Similarly, in the case of expansion in ambient gas the diffusion time of the ablated material through the gas determines the cluster formation time and, hence, the cluster size. Clusters are formed in the dense area near the laser focal spot close to the ablation surface. Cloud of clusters expand and clusters are deposited on substrates and surfaces in the experimental chamber. Depending on the quantity of the ablated material, clusters are deposited on a surface as individual particles or in a form of cluster-assembled foamlike substance. By applying a simple kinetic model we first demonstrate that the formation of clusters is possible in a plume created by a single ultrashort laser pulse. Then we compare the predictions of the model with the experiments where different clusters were produced in vacuum and in ambient gases.

II. GROWTH KINETICS OF CLUSTER FORMATION

We consider a simplified model of nanocluster formation aiming for prediction of the total number of atoms per cluster as function of the average laser plume parameters. The price we pay for such a simplification is the missing information about the internal structure of a cluster. We suggest that a cluster forms via the neutral-to-neutral inelastic sticky collisions and ignore the ion-to-ion, ion-to-neutral, and other complex dusty-plasma collision effects. We assume that the atomic source and the time-dependent density of atoms, the building blocks for the clusters formation $n_1(t)$, are known. Therefore, the number of atoms, their energy and momentum in a plume after the pulse termination are conserved. We also ignore, as a first approximation, the spatial dependence of all quantities, which will be accounted for later on.

Let us assume that clusters are formed by monomer addition in a pair of inelastic (sticky) collisions. We suggest that the first important step on the way to creation of a large cluster is the formation of dimers. Generally a third body is required in a two-body exothermic collision producing a single particle for fulfillment the momentum and energy conservation locally, at the cluster formation spatial point. The third body should be another carbon atom or a cluster. The cross section for atomic collisions that responsible for cluster formation and its internal structure most probably is dangling-bond-direction dependent. Hence, such a cross section itself should be a very complicated function of atomic characteristics, which is unknown to the best of our knowledge. A single cluster formation process, which is three-dimensional (3D) problem with such a cross section, is a formidable task even for a modern-day supercomputer. However, the outcome would be unreliable providing that very little is known about this cross-section function even for the triple collisions. Therefore, we have chosen a different way to solve the problem, where just a total number of atoms per cluster could be predicted as a function of average plume parameters, based on the energy, momentum, and number of atoms conservation in a laser created plume after the end of the pulse. In this approach, the cross section is taken in the form applied for collisions of hard spheres. Thus, the cross section for the cluster containing N atoms is simply proportional to $N^{-2/3}$, as we demonstrate below. In our approach, the coupled rate equations exactly comply with the conservation of the total number of ablated atoms in a plume while the energy and momentum conservation are only implicitly (through the velocity of carbons) coupled to the rate equations. In exact atomic formulation, such coupling should be explicit through the energy and momentum exchange with a third body while in our case the energy and momentum are conserved separately. In our approach therefore the cross section is simply a parameter defining the time for formation

of dimers, trimers etc. as a function of number of atoms per cluster. Comparison to the experiments in Sec. III below demonstrates that the number of particles per cluster as a function of the laser and averaged laser plume parameters can be predicted with sufficient accuracy.

A. Collision cross section

The cross section for atom-atom attachment in a laser plume is unknown. It is reasonable to suggest that attachment cross section is proportional to the elastic one. The cross section for neutral-neutral collision is taken as that for collision of hard spheres. The diffusion coefficient in the mixture of two gases depends on the total cross section σ_{tot}, which expresses as the following:[22]

$$\sigma_{tot} = \frac{\pi}{4}(d_1^2 + d_2^2), \tag{1}$$

where d_1 and d_2 are diameters of particles in the mixture. In case of carbon-carbon scattering $\sigma_{\text{C-C}} = 1.86 \times 10^{-16}$ cm^2 (the covalent radius 0.77 Å; $d_1 = 1.54$ Å). Diffusion of carbon atoms that is the case of cluster formation in ambient gas ($d_{\text{Ar}} = d_2 = 3.76$ Å) depends on $\sigma_{\text{C-Ar}} = 1.3 \times 10^{-15}$ cm^2. In what follows, we suggest that two-atom collisions dominate the formation process (e.g., multiple collisions are neglected). We take into account collisions of N-clusters (cluster containing N atoms) with a single atom only (monomer addition), ignoring the collisions of heavy clusters with each other. The cross section of such an interaction then expresses:

$$\sigma_{N,1} = \frac{\pi}{4}(r_1^2 + r_N^2) \cong \sigma_{1,1} N^{2/3} \quad (N \gg 1),$$

$$r_N \cong N^{1/3} r_1. \tag{2}$$

We assume that the probability of sticky attachment <1 and is proportional to the above atom-to-atom inelastic cross section.

B. Particle conservation law

A set of coupled chemical rate equations for cluster number density n_N (number of N-clusters per unit volume) governs the successive formation of clusters from dimers n_2 to N-clusters. The total number of atoms in all clusters at any time moment in the entire interaction volume should be equal to the total number of single atoms produced by the ablation source:

$$\sum_{i=1}^{N} i n_i = \int_0^t \left(\frac{dn_1}{dt}\right)_0 dt'. \tag{3}$$

It is convenient to present this law also in the form:

$$\sum_{i=1}^{N} i \frac{dn_i}{dt} = \left(\frac{dn_1}{dt}\right)_0. \tag{4}$$

In other words, Eqs. (3) and (4) represent the law of conservation of mass.

C. Formation of clusters by a monomer addition

The set of coupled rate equations describing N-cluster formation in pair sticky collisions then reads:

$$i\frac{dn_i}{dt} = K_{1,i-1} n_1 n_{i-1} - n_i \sum_{k=1}^{i-k} K_{k,i} n_k, \quad i = 2,3, \ldots, N. \tag{5}$$

We remind again that this set of equations represents just the atoms conservation law where the cross section is a parameter proportional to the number of carbons per cluster. The reaction rate conventionally expresses as the following:

$$K_{i,k} = \sigma_{ik} v_{ik}, \tag{6}$$

where v_{ik} is the relative velocity of i cluster and k cluster. The differential equation (5) holds if any arbitrary constant multiplier to reaction rate in Eq. (6) is included. It is assumed that velocity of single atoms $v_1 \gg v_i$ $(i > 2)$, and the collisions between heavier clusters, 2–2; 2–3; 3–3 etc., are ignored because their velocities are lower, $v_N \propto N^{1/2}$. Therefore, the reaction rate for the monomer addition, $K_{1,N} \propto N^{2/3}$, is higher than that for the triple collisions or for pair collisions of larger clusters, $K_{N,N} \propto N^{-5/6}$. The maximum cluster formed comprises N atoms. Then, the coupled set of rate equations reads:

$$2\frac{dn_2}{dt} = K_{11} n_1^2 - K_{12} n_1 n_2,$$

$$3\frac{dn_3}{dt} = K_{12} n_1 n_2 - K_{13} n_1 n_3,$$

$$\ldots$$

$$(N-1)\frac{dn_{N-1}}{dt} = K_{1,N-2} n_1 n_{N-2} - K_{1,N-1} n_1 n_{N-1},$$

$$N\frac{dn_N}{dt} = K_{1,N-1} n_1 n_{N-1}. \tag{7}$$

Applying the particle conservation law Eq. (4) one obtains the equation for the change in time of the number density of building atoms,

$$\frac{dn_1}{dt} = \left(\frac{dn_1}{dt}\right)_0 - K_{11} n_1^2. \tag{8}$$

Equation (8) can be immediately integrated if the source term is known. Afterwards the set Eq. (7) can be successively integrated.

D. Time for the N-cluster formation: Simplified solution

A simple solution for the set of Eq. (6) can be found under the following assumptions. First, it is assumed that the relative velocities are $v_{1,N} \approx v_1$. Second, the attachment cross section expresses as $\sigma_{N,1} \approx \sigma_{1,1} N^{2/3}$; $(N \gg 1)$. We also assume that the number density of constituent atoms is time-independent and $n_1 \gg n_2, n_3, \ldots . n_N$. Then the set Eq. (6) reduces to the following:

$$2\frac{dn_2}{dt} = n_1^2\sigma_{11}v_1 \equiv n_1/t_2, \quad t_2 = (n_1\sigma_{11}v_1)^{-1},$$

$$3\frac{dn_3}{dt} = 2^{2/3}n_2/t_2,$$

$$\cdots$$

$$(N-1)\frac{dn_{N-1}}{dt} = (N-2)^{2/3}n_{N-2}/t_2,$$

$$N\frac{dn_N}{dt} = (N-1)^{2/3}n_{N-1}/t_2. \tag{9}$$

The set of Eqs. (9) can be successively integrated by time to obtain the number density of clusters containing N atoms each,

$$n_N = \frac{n_1}{[(N-1)!]^{1/3}N!}\left(\frac{t}{t_2}\right)^{N-1}. \tag{10}$$

The case under consideration corresponds to $N \gg 1$, thus from the particle conservation follows that $n_N \approx n_1/N$. Thus, Eq. (10) can be reduced to

$$N^{-1} \cong \frac{1}{[N!]^{4/3}}\left(\frac{t_N}{t_2}\right)^N, \tag{11}$$

where t_N is the time necessary for the N-cluster formation. In further simplification the factorial function using the Stirling limit case for $N \gg 1$ reduces to $N! \cong (2\pi)^{1/2}N^{N+1/2}e^{-N}$. Now Eq. (11) transforms into:

$$N \cong e(t_N/t_2)^{3/4}. \tag{12}$$

Inserting the time for the dimer formation t_2 one obtains that the number of atoms per cluster is directly proportional to the number density and velocity of source atoms as the following:

$$N \leq e(t_N n_1\sigma_{11}v_1)^{3/4}. \tag{13}$$

It was implicitly assumed in this derivation that the number density of atomic source n_1 and atomic velocity v_1 are constant during the formation time t_N. In fact, the density spatial distribution in the plume changes from the solid density to zero. Time for N-cluster formation above is actually the time when the plume volume increases to the size L at which its temperature drops down to the limit temperature for the cluster formation. For a one-dimensional adiabatic expansion one gets the formation time $t_N = L/v_1$. Thus the expression in parenthesis in Eq. (13) can be presented as $t_N n_1\sigma_{11}v_1 \cong Ln_1\sigma_{11} = L/l_{mfp} \cong N_{a-a}$, that is the number of atom-atom collisions in a plume; here l_{mfp} is the atomic mean free path in the plume. As the plume atomic density is space dependent, N_{a-a} should be presented in the form

$$N_{a-a} \approx \int_0^L l_{mfp}^{-1}dz = \int_0^L n_1(z)\sigma_{11}dz. \tag{14}$$

One can see that for linear density dependence $n_1(z) = n_0 z L^{-1}$; for the exponential dependence $n_1(z) = n_0 e^{-z/L}$, and for the adiabatic expansion in vacuum $n_1(z) = n_0(1-z/L)^{2/(\gamma-1)}$ the number of collisions differs only by numerical coefficient of the order of unity ($b = 0.25-0.63$), which we leave as a fitting parameter:

$$N_{a-a} b n_0 \sigma_{11} L, \tag{15}$$

here n_0 is the initial density of the target. Formula (15) indicates clearly the dominant contribution of the dense parts of the plume to the cluster formation process. Now, the number of atoms per cluster expresses as the following:

$$N \cong eN_{a-a}^{3/4} = B(n_0\sigma_{11}L)^{3/4}. \tag{16}$$

Here $B = eb^{3/4}$ is the fitting coefficient that should be extracted from the comparison to the experiments (B changes within the range of 0.96–1.92).

E. Number and temperature of ablated carbon atoms

In what follows, we apply the above model to cluster formation by a single pulse and estimate the cluster size as a function of laser parameters. The cluster formation scenario is as follows. First, the flow of hot carbons is created during ablation. The laser pulse duration is too short for the clusters to be formed during the pulse. Therefore, after the end of the pulse the ablated vapor either diffuses, when the chamber is filled with a gas, or adiabatically expands into vacuum. The total number of atoms ablated per pulse N_{abl} and their initial temperature T_0 define the initial conditions for the plume expansion accompanied by the cluster formation. The number of ablated atoms is $N_{abl} = n_0 V_0 \equiv n_0 S_{foc} l_{abl}$; here S_{foc} is the focal spot area, n_0 is a number density of a target, l_{abl} is the ablation depth, and V_0 is the ablated volume.

To promote effective cluster formation process the laser plume has to be in a highly collisional state, which in turn requires high-ablation rate and thus reasonably high laser ablation fluence well above the ablation threshold. We assume that in these conditions the target material is at least single ionized and the electron C_e and ion C_i specific heat can be taken as for the ideal gas: $C_e = C_i = 3k_B/2$. We also suggest that at the beginning of the plume expansion the temperatures of electrons and ions are equilibrated. Thus, the maximum initial energy per atom at the beginning of expansion reads

$$T_0 = \frac{2(F_a - F_{thr})}{3n_a l_{abs}}, \tag{17}$$

where F_a and F_{thr} are respectively the absorbed and the threshold laser fluence, and l_{abs} is the absorption depth in the target material. The ablation threshold reads[21]

$$F_{thr} \cong \frac{3}{4}\frac{n_a l_{abs}(\varepsilon_b + J_i)}{A}. \tag{18}$$

Here ε_b is the binding energy and J_i is the first ionization potential. For ablation of graphite target as a source of carbon atoms ($A \sim 0.85$, $l_{abs} \sim 30$ nm, $\varepsilon_b + J_i \sim 15$ eV, and $n_a = 10^{23}$ cm^{-3} for graphite) one gets the threshold $F_{thr} = 0.8$ J/cm^2.

The ablated depth can be expressed as the average between two limiting cases, $l_{abl}^{n-eq} < l_{abl} < l_{abl}^{\max}$ where the limits

are determined by the nonthermal (nonequilibrium) mode of ablation.[21] The maximum ablation depth $l_{abl}^{\max}$ is defined by the condition that all the absorbed laser energy spent on breaking bonds and the kinetic energy of ablated atoms is zero:

$$l_{abl}^{\max} = \frac{F_a}{n_a(\varepsilon_b + J_i)}. \tag{19}$$

The lower limit for the ablation depth l_{abl}^{n-eq} is determined by a condition that the kinetic energy of ablated atoms is maximum, $l_{abl}^{n-eq}=0.5l_{abs}\ln(F_a/F_{thr})$.

Let us compare these results with the experimental data. The ablation depth can be estimated from the measured ablated mass m_{abl} per single pulse,

$$l_{abl}^{\exp} = \frac{m_{abl}}{S_{foc}\rho}.$$

Taking the incident laser fluence of 8 J/cm^2, which is ten times higher than the ablation threshold, and the absorption $A=0.85$ ($F_a=6.8$ J/cm^2) one gets $l_{abl}=160$ nm, which is in qualitative agreement with the experimentally measured 200 nm—see Fig. 1 below in Sec. III B.[23] The ion temperature at the beginning of expansion for the same parameters is $T_0=21.3$ eV.

F. Expansion-limited aggregation in adiabatically expanding plume of a single pulse

Let us assume that the ablated plume adiabatically expands after the end of the pulse in vacuum as an ideal gas with the adiabatic constant γ, $T=T_0(V_0/V)^{\gamma-1}$. We suggest that clusters can be formed in an expanding plume during the period when the carbon temperature exceeds the minimum temperature for cluster formation, $T_{\min}=T$. The plume volume at that instance reads[24]

$$V_{\max} = V_0(T_0/T_{\min})^{1/(\gamma-1)}. \tag{20}$$

There are two possible scenarios of expansion depending on the experimental conditions: plume propagation in one-dimension (plane-wave expansion) or in three-dimensions (hemispherical expansion). At the initial expansion stage when the dense plume thickness is much less than the focal spot size, which of the order of tens of microns, the expansion is well approximated as one dimensional: $V_{\max}=S_{foc}L_{\exp}$ and $V_0=S_{foc}l_{abl}$. The expansion length from Eq. (20) expresses as follows:

$$L_{\exp}^{(1D)} = l_{abl}(T_0/T_{\min})^{1/(\gamma-1)} \propto l_{abl}F_a^{1/(\gamma-1)}. \tag{21}$$

In 3D-expansion case $V_{\max}^{(3D)}=\frac{4\pi}{3}L_{\exp}^3$, $V_0=S_{foc}l_{abl}$, and $r_0=(\frac{3S_{foc}l_{abl}}{4\pi})^{1/3}$ as for an ideal gas $\gamma=5/3$ the expansion length reads:

$$L_{\exp}^{(3D)} = r_0\left(\frac{T_0}{T_{\min}}\right)^{1/2} \propto l_{abl}^{1/3}F_a^{1/2}. \tag{22}$$

Note that the 3D-expansion length is in accord with hydrodynamic solution for adiabatic expansion.[24] Now one can also calculate the cluster radius, $r_{cl}=(3N/4\pi n_0)^{1/3}$, with the help of Eq. (16) and assuming that the cluster material density is known,

$$r_{cl} = (3N/4\pi)^{1/3}n_0^{-1/12}(\sigma_{11}L_{\exp})^{1/4}, \tag{23}$$

which shows very weak dependence on the material density. We suggest that the minimum temperature for formation of carbon clusters equals to the temperature of graphitization of $\sim 1,200$ K$=0.1$ eV.

Experiments at low pressure of 20 mTorr, which we can consider as experiments in vacuum (the atomic mean free path is comparable to the target-substrate distance), with $S_{foc}=10^{-5}$ cm^2, $F_a=6.8$ J/cm^2, ablation depth of 200 nm, $\sigma_{\text{C-C}}=1.86\times10^{-16}$ cm^2, and $T_0=21.3$ eV) correspond to 3D-expansion because $L_{exp}\gg r_{foc}$ at these parameters in accord with Eq. (22). By applying these parameters to the Eq. (22) along with Eq. (23) and taking numerical coefficient $B=1$, the cluster diameter is 2.68 nm, that agrees qualitatively well with the measured average diameter of 3.2 ± 0.5 nm.

One should note that the attachment probability, as well as the minimum temperature for the cluster formation are unknown to the best of our knowledge. Those parameters were suggested above on the basis of general laws as well as several approximations.

G. Diffusion limited aggregation: cluster growth in ambient gas

Growth of clusters in the ambient gas was conceived as a basic process for any cluster formation process. Use of an ambient gas has the advantages of a confinement that increases the lifetime of constituent atoms in formation region and therefore increasing the probability of sticky attachment. On the other hand the ambient gas acts as a heat sink decreasing the temperature necessary for cluster formation. This was the reason for heating the argon gas to 1200–1600 °C during the nanotube growth by the laser ablation process.[1] Another limiting factor is that the pressure of the ambient gas cannot be increased over the threshold for optical breakdown thus decreasing the ablation rate.

The shock wave forms and propagates into the gas immediately after the laser pulse. The shock front however is smeared over a distance comparable to the carbon mean-free path in a gas $l_{mfp}=(n_{\text{Ar}}\sigma_{\text{C-Ar}})^{-1}$. For the 50–1000 Torr argon pressure the density range is $n_{\text{Ar}}=3\times10^{18}-6\times10^{19}$ cm^{-3}. The mean-free-path range $l_{mfp}=(0.15-3.33)\times10^{-4}$ cm is longer than the ablation depth, which is the thickness of the energy deposition region. Diffusion therefore dominates, and thus we ignore the shock wave stage in our future estimates.

Let us first obtain the maximum diffusion length from condition that cluster formation stops at some temperature $T_{\min}$. We assume that carbons cooling proceeds in two overlapping stages: nearly adiabatic expansion and additional cooling due to carbon-argon collisions. At the adiabatic expansion stage the plume cools down to the temperature $T_C=T_0(\frac{r_0}{L_D})^2$, here $r_0=(\frac{3S_{foc}l_{abl}}{4\pi})^{1/3}$. Correspondingly, the carbon density at the same moment expresses as $n_C=n_0(\frac{r_0}{L_D})^3$. The temperature in the carbon-argon mixture after equilibration is then $T_{\text{mix}}=T_C(\frac{n_C}{n_{\text{Ar}}+n_C})$. Now, the maximum diffusion length

for the cluster formation zone can be defined from the condition that the temperature in the mixture equals to the minimum temperature for the cluster formation $T_{mix}=T_{min}$, which expresses by algebraic equation,

$$T_{min}=\frac{T_0 n_C}{(n_{Ar}+n_C)}\left(\frac{r_0}{L_D}\right)^2. \quad (24)$$

By introducing the variable $x=L_D/r_0$, the above equation takes the form

$$x^2\left(1+x^3\frac{n_{Ar}}{n_0}\right)=\frac{T_0}{T_{min}}. \quad (25)$$

In the pressure range $P_{Ar}=50-1000$ Torr argon number density is in the range $n_{Ar}=(3-60)\times 10^{18}$ cm^{-3}. As can be seen from the above equation, the influence of ambient gas on the diffusion length of the ablated carbons ($n_0=10^{23}$ cm^{-3}) becomes significant when the gas pressure approaches 10% of the atmospheric pressure. One can present solution of Eq. (25) for two limit cases: diffusion-dominated expansion, $n_{Ar}\gg n_C$, and the opposite limit corresponding expansion into vacuum:

$$L_D\approx r_0\left(\frac{T_0}{T_{min}}\right)^{1/5}\left(\frac{n_0}{n_{Ar}}\right)^{1/5}, \quad n_{Ar}\gg n_C,$$

$$L_{vac}=r_0\left(\frac{T_0}{T_{min}}\right)^2. \quad (26)$$

Let us calculate now the cluster size in conditions when diffusion dominates. Diffusion of single carbons in argon of density n_{Ar} proceeds with diffusion velocity, $D=lv_C/3\approx v_C/(3n_{Ar}\sigma_{C\text{-}Ar})$, where $\sigma_{C\text{-}Ar}$ is the cross section for carbon-argon elastic collisions, which is taken the same as that for the hard sphere collisions. Note that C-Ar collision cross section is almost 10 times larger than that for C-C collisions. The time for N-cluster formation now equals to diffusion time:

$$t_N\equiv t_D=\frac{L_D^2}{D}=\frac{3n_{Ar}\sigma_{C\text{-}Ar}L_D^2}{v_C}. \quad (27)$$

The carbon-carbon collision time reads: $t_{11}=(n_C\sigma_{C\text{-}C}v_C)^{-1}$; here v_C is carbon atom velocity and $n_C=n_0(\frac{r_0}{L_D})^3$ as above. Then, the number of atoms in N-atoms cluster in accord with Eq. (12) reads

$$N\cong e(t_N/t_2)^{3/4}=C_1(n_{Ar}\sigma_{C\text{-}Ar}\sigma_{C\text{-}C}n_0r_0^3/L_D)^{3/4}. \quad (28)$$

Now the cluster radius, $r_{cl}=(3N/4\pi n_0)^{1/3}$, as a function of target and gas parameters for the diffusion-dominated growth immediately follows:

$$r_{cl}\approx C_2n_0^{-1/12}r_0^{3/4}(n_{Ar}\sigma_{C\text{-}Ar}\sigma_{C\text{-}C})^{1/4}L_D^{-1/4}, \quad (29)$$

where C_1 and C_2 are dimensionless numerical coefficients that should be extracted from the experiments. Finally we present an explicit scaling of the cluster radius in the expansion-limited aggregation conditions in the following form:

$$r_{cl}\approx C_2n_0^{-2/15}r_0^{1/2}n_{Ar}^{3/10}(\sigma_{C\text{-}Ar}\sigma_{C\text{-}C})^{1/4}\left(\frac{T_{min}}{T_0}\right)^{1/20}. \quad (30)$$

However at a pressure close to that of the atmospheric pressure and with laser intensity in excess of 10^{13} W/cm^2 conditions are close to those for the optical breakdown of argon.[25] Therefore, there is a dependence on the buffer gas pressure hidden in the ablation depth (that enters in r_0). Experiments demonstrated that strong decrease of ablation depth occurs at a pressure exceeding 100 Torr. Thus, the cluster radius scales up with the buffer gas density, the cross section, and the ablation depth in the diffusion dominated conditions as the following:

$$r_{cl}\approx C_2n_0^{-2/15}l_{abl}^{1/6}n_{Ar}^{3/10}(\sigma_{C\text{-}Ar}\sigma_{C\text{-}C})^{1/4}\left(\frac{T_{min}}{T_0}\right)^{1/20}. \quad (31)$$

As one can see from Eq. (31), the cluster size is a very weak function of the plume temperature and the initial target density. The main factor is the density of the ambient gas, which affects the size approximately as a cubic root of the gas pressure.

III. NANOCLUSTER GROWTH EXPERIMENTS IN AMBIENT GAS AND IN VACUUM

A. Laser ablation conditions and diagnostics

Carbon nanofoam samples were produced using a high power frequency doubled Nd:YVO_4 laser system consisted of an oscillator and power amplifier, generating an average power up to 41 W in 12 ps pulses at a wavelength of 532 nm and MHz-range repetition rate.[26] The oscillator was configured as a passively mode-locked system with an extremely long resonator length up to 100 m.[27] This passive mode locking was achieved via the use of a saturable absorption mirror (SESAM), and the long-resonator length was arranged using a multipass cell. Various configurations of this multi-pass cell enabled the oscillator to operate at repetition rates of 1.5, 2.7, 4.1, and 28 MHz. Lower repetition rates down to 150 kHz were also obtained with the use of an acousto-optic switch. The repetition rate flexibility was especially designed to enable variable single pulse energy of the laser, which could be changed in the range from 0.1 μJ/pulse to 10 μJ/pulse.[26] In order to achieve constant ablation conditions on the target surface, a high degree of control over the scanning of the focused laser beam should be maintained. A computer-controlled positioning system was designed and built in house, such that one could generate arbitrary scanning patterns with a high degree of accuracy, area coverage uniformity, and constant scanning velocity.[28] The laser beam was focused down to a 15 μm spot onto a graphite target placed in a vacuum chamber which could be filled with various gases. With the maximum average laser power of ~40 W this produced incident intensity of 1.2×10^{12} W/cm^2 with corresponding fluence of 15 J/cm^2 at the repetition rate of 1.5 MHz.

The chamber was pumped to the vacuum level ~1 mTorr, and the gas pressures were varied from 20 mTorr to 1500 Torr (2 atm) in the experiments. The mean-free path

of hot carbon atoms in argon at the pressure of 50 mTorr is of the order of 10 cm, larger than the target-to-substrate distance. For this reason, there is no carbon-to-argon collisions, and thus we consider as vacuum conditions in the chamber at the pressure of <50 mTorr. The background gas was leaked through the chamber at a flow rate of 200–300 sccm keeping the pressure constant by a vacuum pump. The results for cluster size distribution were produced for cluster samples made in various experimental conditions such as different background gas type (He, Ar, Kr, and Xe) and background gas pressure.

B. Ablation rate and ablation threshold measurements

Ablation threshold was experimentally defined as the particular laser fluence at which a single atomic layer was removed from the target.[16,29] The ablation rates of carbon targets have been measured by performing a series of ablation experiments lasting 60 s, with a scanned laser beam, across a range of fluences. The amount of material ablated was measured by weighing the sample before and after ablation with accuracy 10^{-4} g at each laser fluence. The amount of material ablated from a single laser pulse m_{avg} (g) was found by averaging the total ablated mass over the total number of laser pulses. The error due to the redeposition of ablated material back onto the target surface was within few percent only as the diffusion process is predominantly monodirectional away from the target surface in high-repetition-rate laser ablation. At 1.5 MHz and for ablation lasting 60 s, for example, the total number of laser pulses was 9×10^7. The ablation depth, d_{abl} (cm) per single pulse is $d_{abl}=m_{avg}/(s_f\rho)$, where s_f is the laser spot area in cm^2 and ρ is the target material density in $(\mathrm{g/cm}^3)$.[19] The ablation rates at various fluences are presented in Fig. 1. The threshold was defined as the laser fluence at which the ablation depth per pulse was equal to the thickness of a single atomic layer in graphite (Fig. 1). The covalent σ bond with length 1.46 Å has the highest strength (524 kJ/mol), while the π bond is a much weaker van der Waals bond (7 kJ/mol) with a length of 3.34 Å. Hence, in the context of full atomization in the plume, the in-plane covalent σ-bond length is used to define the ablation threshold.

The ablation threshold fluence in the presence of argon at atmospheric pressure was found to be 0.23 $\mathrm{J/cm}^2$. This value is significantly lower than the 0.8 $\mathrm{J/cm}^2$ predicted by Eq. (18) above, which does not take into account the existence of ambient gas. The discrepancy between the prediction Eq. (18) for vacuum and the experimental results obtained in argon can be accounted by considering the role of the buffer gas as in the ablation process, which stimulates thermal evaporation after the laser pulse.[29,30]

The ablation rate in terms of the number of atoms ablated per pulse N_{abl} can be calculated as $N_{abl}=d_{abl}s_{foc}n_a$, where s_{foc} is the laser spot area. In this case the ablation rate in Fig. 2 at 8 $\mathrm{J/cm}^2$ translates to approximately $N_{abl}\sim10^{13}$ atoms per pulse. The efficiency of nanocluster formation in the typical experimental laser ablation conditions, i.e., at 25–40 W laser power, 1.5 MHz repetition rate, 8 $\mathrm{J/cm}^2$, 50 Torr of Ar, was on the order of 0.5 g of nanomaterial per hour.[31–33]

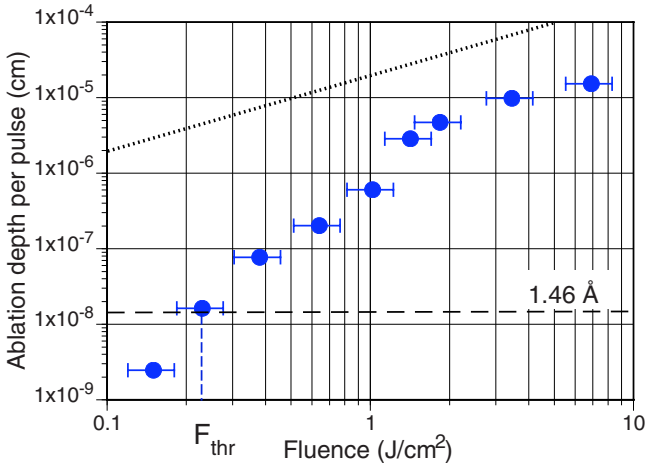

FIG. 1. (Color online) Ablation rate measurement for graphite in argon at atmospheric pressure. The characteristic atomic spacing of 1.46 Å is represented by the dashed line. The intersection of a fitting curve with the line determines the ablation threshold fluence of 0.23 $\mathrm{J/cm}^2$ for graphite at atmospheric pressure. The dotted line above the experimental points is the maximum possible ablation rate followed from the law of conservation of energy Eq. (19).

As the pressure is increased, ablation becomes less efficient due to laser scattering from the laser plume. At 300 Torr the number density of gas fill atoms is $\sim1.8\times10^{19}$ cm^{-3} that is comparable to the density of carbons in the ablated plume. However, another effect becomes increasingly important in the ablation process with the rising gas pressure, namely, the optical breakdown of the buffer gas. An estimate of the rise of the electron density in the plume through the avalanche ionization and multiphoton ionization processes show that it takes about two picoseconds to reach the critical plasma density at 10^{12} $\mathrm{W/cm}^2$ for 532 nm laser.[25,31] The plasma formation in the gas results in significant decrease in laser absorption and in the consequent decrease in the ablation rate. The rate measurements showed the ablation rate decreases almost five times as the pressure increases from 300 to 1500 Torr.

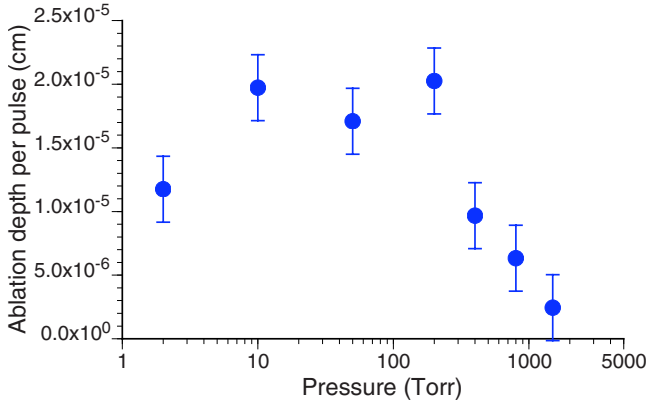

FIG. 2. (Color online) Ablation rate vs pressure of argon gas for graphite at the laser fluence 8 $\mathrm{J/cm}^2$.

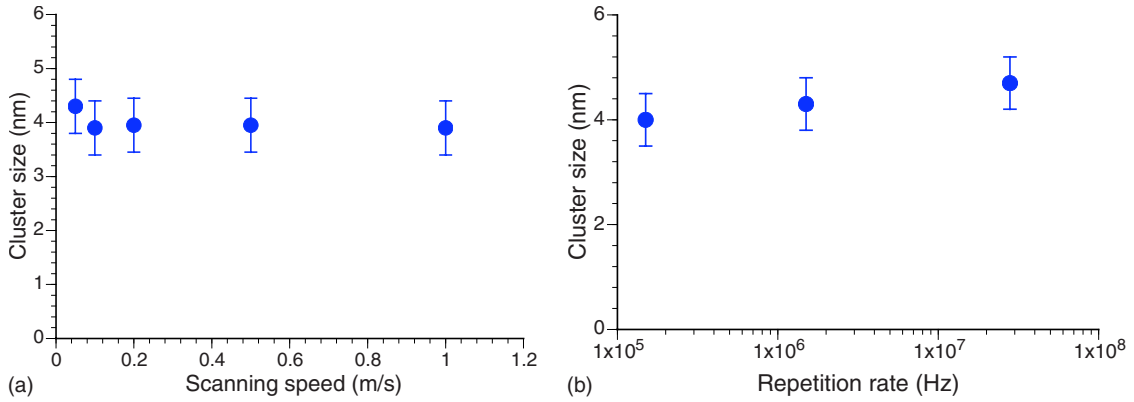

FIG. 3. (Color online) Average cluster size in different experimental conditions: (a) the scanning speed variation at a fixed 1.5 MHz repetition rate; (b) the repetition rate variation at a fixed scanning speed of 1 m/s. Error bars are ± 0.5 nm. The results show very slow or absence in the average cluster size variation.

C. Carbon cluster formation experiments

A series of experiments were conducted to investigate the dependence of the cluster size upon various experimental parameters. These parameters included the laser scanning speed, three different repetition rates of 150 kHz, 1.5 MHz, and 28 MHz; the background pressure variation in experiments with argon in the range from 20 mTorr to 1500 Torr, and the use of different chamber filling gases at a fixed pressure of 50 Torr.

Results pertaining to the average cluster sizes of the different nanofoam samples were obtained from transmission electron microscope (TEM) images taken of carbon nanofoam created in different laser and chamber parameters. The foam was deposited upon copper TEM grids, which had been coated with holey carbon films (hole size of 10–1000 nm). Short exposures (less than 10 s) were performed in order to coat the TEM grid, located approximately 1 cm from the target, to ensure individual clusters could be seen as-deposited in the web-like arrangement, which arises due to the propagation of clusters through the background gas. Cluster size distributions were obtained using a series of ten TEM images taken at magnifications of 300–400 k, and about 500 ± 100 clusters were measured to generate a cluster size distribution. The results were then fitted with a best-fit Poissonian distribution to obtain an indication of the average size. The size distributions in various experimental conditions are presented below.

1. Size independence on the scanning speed and the laser repetition rate

The experiments demonstrated that there was little if any significant difference in measured average cluster size for changes in the scanning speed on the range from 0.05 m/s to 1.0 m/s and with the laser repetition rate from 150 kHz to 28 MHz [Figs. 3(a) and 3(b)], both at 50 Torr of Ar pressure. For this reason all the further experimental tests were conducted with the repetition rate of 1.0 m/s and at 1.5 MHz rate.

The scanning speed of 1 m/s of the focal spot of 15 μm diameter at the 1.5 MHz laser repetition rate means that in average 22 laser pulses hit the same point on the target surface. The theory presented in Sec. II above suggests that the plume expansion time (coinciding with the cluster formation time) is less than 10 ns. Therefore, one should not expect the accumulation effect due to 36 ns time gap between the consecutive pulses at 28 MHz repetition rate. The observed independence of the cluster size on the scanning speed is the indirect confirmation of the fact that the cluster formation time is less the 36 ns between the pulses.

In addition, we analyzed the cluster size distribution at various distances from the target surface, namely, with a collecting TEM grid located at 1, 3, 5, 10, and 20 mm. There was no variation found in the average cluster size within the experimental error of ± 0.5 nm. These results indicate that the cluster growth process takes place in close vicinity of the ablation area below 1 mm and that the average size of the nanoparticles does not change in further diffusion through the buffer gas.

2. Size dependence on the buffer gas pressure

The size distributions of nanoclusters were measured and analyzed at pressures starting from 0.2 Torr and higher, approaching, and exceeding the atmospheric pressure. Some typical TEM images are presented in Fig. 4, and the size distributions at various pressures are in Fig. 5. There is a noticeable increase in an average cluster size (maximum of

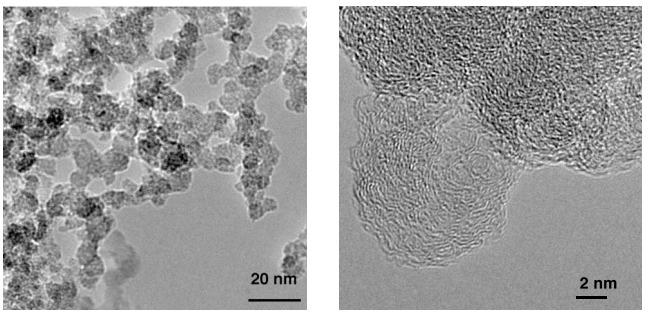

FIG. 4. Typical TEM images of carbon nanofoam material with the average cluster size of (a) 5.5 nm and a single nanocluster of (b) ~ 10 nm.

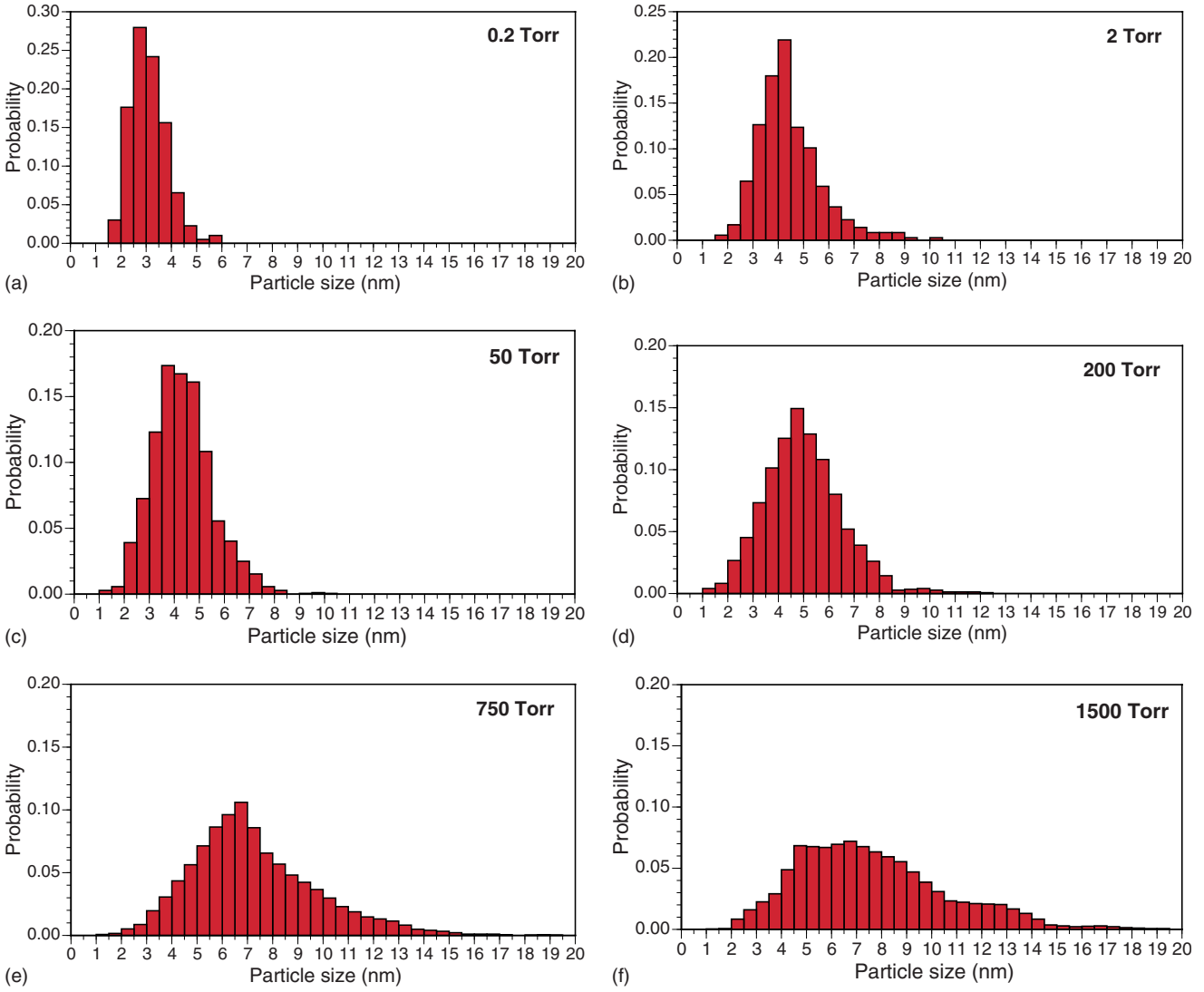

FIG. 5. (Color online) Examples of cluster size distributions at various Ar pressures from 0.2 to 1500 Torr. There is a noticeable broadening of the size distribution as well as the growing large size tail with increase of pressure.

distribution) as well as in the large-cluster tail of the size distributions measured at pressures in excess of 50 Torr. The average size of a cluster shows only a weak dependence with increasing pressure while the number of larger clusters in the tail grows faster than the average size. The results show the tendency of broadening the distribution curve, and the growing tail of large cluster sizes with increase of buffer gas pressure.

Figure 6 represents the average size distributions of clusters produced at pressures approaching and exceeding atmospheric pressure. Clearly there is a noticeable increase with pressure, especially at pressures in excess of 50 Torr. At such pressures the density of carbons in the ablated plume is on the order of 10^{19} cm^{-3}, which is comparable to the number density of the buffer gas atoms. The diffusion through the buffer gas dominates the growth process above this pressure. It was noted that the maximum size increases faster than the average size with pressure increase: the average size increases with pressure by way of $n_{\mathrm{Ar}}^{0.2}$ while maximum cluster size increases as $n_{\mathrm{Ar}}^{0.3}$ as it is predicted by Eq. (30). The re-

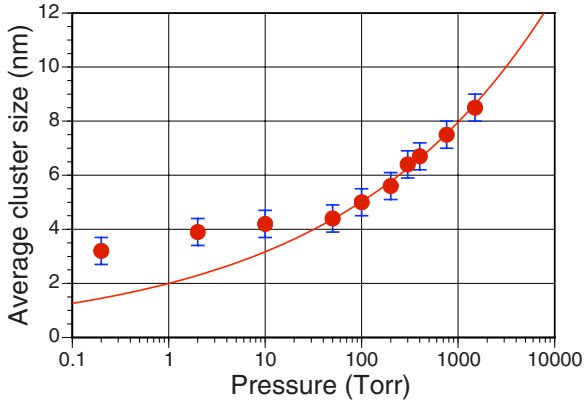

FIG. 6. (Color online) Average cluster size at various pressures. The error bar is the accuracy of the cluster size measurements of ± 0.5 nm. A solid curve is $r_{cl} \propto n_{\mathrm{Ar}}^{0.2}$. The laser fluence was 8 J/cm^2 in all experiments.

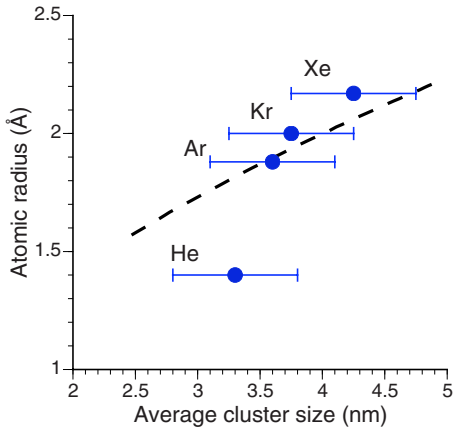

FIG. 7. (Color online) Average cluster size in different gas environment at 50 Torr pressure. The dashed line is a square root scaling based on Eqs. (30) and (31).

sults in Fig. 2, however, show that ablation becomes less efficient as the pressure increases due to increased ionization and, as a consequence, increased scattering from a denser and more ionized laser plume. As a result of the lowered ablation rate, the two competing factors of increased confinement and lower feedstock of ablated material from the target to the cluster formation zone result in a reduced dependence of the cluster size upon pressure.

In the pressure range below 50 Torr where the plume density exceeds the buffer gas density the cluster growth process is determined by the plume expansion. There is no significant influence of the gas pressure on the cluster growth process in the expanding carbon plume. Only small change in the average size from 3.2 ± 0.5 to 4.4 ± 0.5 nm was observed for the pressure range 0.2–50 Torr. The size distribution was much narrower in the expansion-limited aggregation of nanoclusters below 50 Torr when compared to the diffusion-limited aggregation in the pressure range above 50 Torr.

3. Size dependence on the buffer gas

The average size measurements for cluster size distributions produced in He, Ar, Xe, and Ne as buffer gases at the same pressure of 50 Torr are presented in Fig. 7. It is clear from the data that there is a small but noticeable difference in measured average cluster size for different buffer gases.

The theory developed in Sec. II above predicts that the main influence of the buffer gas on the cluster size relates to the increase in the attachment cross section [see Eqs. (30) and (31)], which is directly proportional to the atomic cross section of a buffer gas. This cross section is proportional to the square of atomic radius, $\sigma \propto r^2$. The atomic radius of the inert gases increases from 1.40 Å for He, to 1.88 Å for Ar, to 2.02 Å for Kr, and to 2.17 Å for Xe.[34,35] The cluster size changes with the cross section as $r_{cl} \propto \sigma^{1/4}$. Therefore, we can estimate the expected cluster radius increase from the formation, for example, in helium ($r_{\mathrm{He}}=1.40$ Å) to the formation in xenon ($r_{\mathrm{Xe}}=2.17$ Å) in similar ablation conditions as $r^{cl}_{\mathrm{Xe}}/r^{cl}_{\mathrm{He}} \propto (r_{\mathrm{Xe}}/r_{\mathrm{He}})^{1/2}=1.24$. This ratio is close to the experimentally measured $r^{cl}_{\mathrm{Xe}}/r^{cl}_{\mathrm{He}}=1.29$. The cluster sizes estimated from other gas radii yields even closer predictions for the experimental values.

4. Cluster growth in expanding plume in vacuum

In the low-pressure range below 50 Torr the gas pressure has little effect on the average cluster size (Fig. 6) as the gas pressure is below the density in the hot expanding laser plume. In our experiments, vacuum was considered to be the case in which the mean free path in the experimental chamber is greater than the distance from the target to the substrate. At the lowest pressure of 20 mTorr used in the experiments the mean free path of gas atoms at room temperature is about 10 mm, which was greater than the 5 mm target-to-substrate distance. For this reason, this pressure effectively represented the conditions of the ablated plume expanded into vacuum.

Figure 8 presents TEM images depicting the transitional nature of material deposition as the pressure is increased from effective vacuum of 20 mTorr to 2 Torr. Clearly for the vacuum situation (pressure 20 mTorr) in the left image, the holey carbon grid is coated with a thin solid layer; however, closer inspection reveals that the film is composed of aggregated clusters similar in size to those observed in the presence of a background gas. These clusters are visible around the edges of the film, where the contrast is great enough for them to stand out. In the middle image, the pressure has been increased to 200 mTorr and it is clear now that the presence of a buffer gas is beginning to introduce a more foamlike appearance to the deposited material due to the presence of collisions as the plume propagates to the substrate. Finally, the image on the right shows material produced at 2 Torr displaying the expected structure achieved through deposition of clusters in the presence of a background gas.

As the pressure is increased from vacuum toward a few Torr, the presence of the background gas now serves to in-

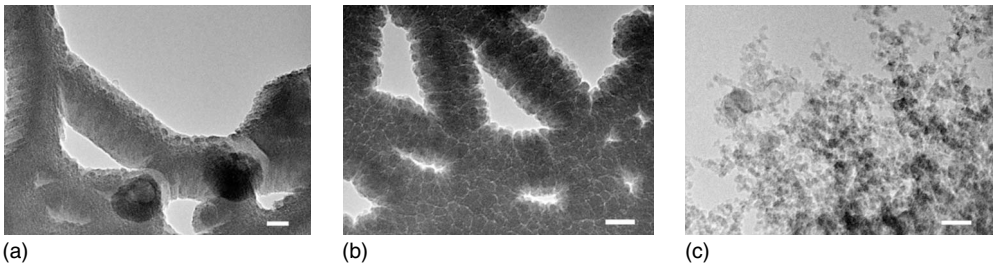

FIG. 8. TEM images of carbon nanocluster formed material created at various pressures. From left to right the images depict material created at 20 mTorr, 200 mTorr and 2 Torr, respectively. Scale bars are 25 nm in all images.

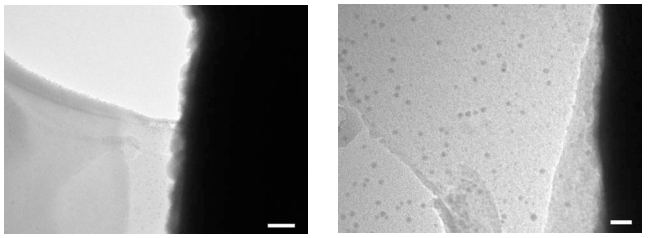

FIG. 9. TEM images of deposited material in vacuum (20 mTorr). Left, low-magnification image shows a region in the center shadowed from the ablation source by the edge of a copper TEM grid, while the right image is a magnified area with clearly seen individual nanoclusters produced in the plume expanding into vacuum. The scale bars are 100 nm in the left image and 25 nm in the right one.

duce a transition between thin solid film formation on the substrate and foam formation, by diffusing the clusters through the gas. The resulting weblike product is seen in the right hand image of Fig. 8.

To say with certainty that the clusters seen in vacuum are the same as those seen in the presence of a buffer gas requires cluster size distributions to be created for both cases. Hence, clusters need to be found in vacuum deposited individually upon substrates. Such clusters could be found on grids in shadowed areas where ablated carbon material could not be deposited directly. The low-magnification image on the left of Fig. 9 shows a region, in the center of the image, shadowed from the ablation source by the edge of a copper TEM grid where clusters were individually deposited on the holey carbon film.

IV. DISCUSSION AND CONCLUSIONS

We developed a simple kinetic theory for nanoparticles growth in a laser plume in various buffer gas conditions which predicts the following growing characteristics observed in the experiments.

(i) Nanocluster growth process takes place in a relatively short time below 10 ns in a laser-ablated plume produced by a single laser pulse. This conclusion was indirectly supported by experiments where the nanocluster average size was not changed with the laser repetition rate increasing from 150 kHz up to maximum 28 MHz, where the time gap was reduced to 36 ns.

(ii) The buffer gas pressure has two distinguished regions affecting the cluster size. At the pressure range below ~50 Torr the number density of atoms in the plume is higher than in the background gas and the effect of confinement of the laser plume is negligible. The cluster growth process in the plume is determined by the collisions between the ablated atoms, which we term as *expansion-limited aggregation* of nanoclusters. This conclusion was supported by experimental observation of nanocluster growth in vacuum conditions, and by a very weak, if any, cluster size dependence on buffer gas pressure at the pressure range below 50 Torr. As soon as it has formed in the expanding plume, there is no further size increase while the cluster diffuses through the buffer gas.

(iii) In the pressure range above ~50 Torr the kinetic theory provides a semiquantitative agreement between the predicted and the measured cluster size dependence on gas pressure. In this high-pressure range the process of growth is usually referred to as *diffusion-limited aggregation* of nanoclusters.[36]

(iv) The developed kinetic approach closely predicts, for the first time to our knowledge, the dependence of the cluster size on the type of gas used in the experiments. The size is mainly determined by the collisional cross section of the gas atoms.

The cluster formation occurs by a monomer addition, i.e., by atom-to-atom or atom-to-cluster collisions, in a space close to the ablation surface in a few nanoseconds time after the laser pulse. The cluster size is controlled by the plume expansion time in vacuum, or by atomic diffusion in the ambient gas in the pressure range above the ablated plume density. This time in turn is explicitly connected to the laser, target material, and filling gas parameters. Experimental studies and analysis of the results show that a single ultrashort pulse of ~100 fs duration can produce a few nanometer small clusters with a very weak dependence on the laser fluence and the ambient gas type or pressure.[37,38]

The theory is applicable for the cluster formation from any mono-atomic material. We demonstrate this by applying the presented theoretical treatment to the formation of silicon nanoclusters in vacuum with a 780 nm 120 fs laser focused on a silicon surface to produce laser fluence of 5 J/cm^2. The theory predicts the average cluster diameter of 6.9 nm, which is in good agreement with the experimental observations of 8 ± 2 nm.[14]

The developed here theoretical analysis supported by the experimental results shows that the ultrashort laser pulses could be applied for producing nanoclusters of different materials with cluster size below the critical value of 3–5 nm, depending on the material, which separates the nanoproperties from those of the material in a bulk. The cluster size can be controlled mainly by the change in the ambient gas pressure in combination with the laser fluence. Decent example of formation of small carbon nanoclusters with unusual properties is the production of all-carbon nanofoam assembled from 4 to 6 nm clusters possessing strong paramagnetic properties opposite to a diamagnetic carbon in bulk.[33,39,40] One can produce nanoclusters with predictable and experimentally controllable size in a range of 3–10 nm by single femtosecond pulses with the fluence of 5–10 J/cm^2.

ACKNOWLEDGMENTS

The support of the Australian Research Council through the Discovery Program and WPI Center for Materials Nanoarchitectonics (MANA-NIMS) are gratefully acknowledged.

*gam111@rsphysse.anu.edu.au
†Present address: Australian Patent Office, Woden, Australian Capital Territory 2606, Australia.

[1] *Carbon Nanotubes: Preparation and Properties*, edited by T. W. Ebbesen (CRC, Boca Raton, 1997).
[2] P. Milani and S. Iannotta, *Cluster Beam Synthesis of Nanostructured Materials* (Springer, Berlin, 1999).
[3] T. W. Ebbesen and P. M. Ajayan, Nature (London) **358**, 220 (1992).
[4] E. G. Gamaly and A. V. Rode, in *Encyclopaedia of Nanoscience and Nanotechnology*, edited by H. S. Nalwa (American Scientific, Stevenson Range, 2004), Vol. 7, pp. 783–809.
[5] V. E. Bondybey and J. H. English, J. Chem. Phys. **76**, 2165 (1982).
[6] S. J. Riley, E. K. Parks, C. R. Mao, L. G. Pobo, and S. Wexler, J. Phys. Chem. **86**, 3911 (1982).
[7] M. Ullmann, S. K. Friedlander, and A. Schmidt-Ott, J. Nanopart. Res. **4**, 499 (2002).
[8] R. E. Smalley, Laser Chem. **2**, 167 (1983).
[9] H. W. Kroto, J. R. Heath, S. C. O'Brien, R. F. Curl, and R. E. Smalley, Nature (London) **318**, 162 (1985).
[10] S. Iijima, Nature (London) **354**, 56 (1991).
[11] D. Golberg, Y. Bando, M. Eremets, K. Takemura, K. Kurashima, and H. Yusa, Appl. Phys. Lett. **69**, 2045 (1996).
[12] W. Marine, L. Patrone, B. Luk'yanchuk, and M. Sentis, Appl. Surf. Sci. **154-155**, 345 (2000).
[13] L. Patrone, D. Nelson, V. I. Safarov, M. Sentis, W. Marine, and S. Giorgio, J. Appl. Phys. **87**, 3829 (2000).
[14] S. Amoruso, R. Bruzzese, N. Spinelli, R. Velotta, M. Vitiello, X. Wang, G. Ausanio, V. Iannotti, and L. Lanotte, Appl. Phys. Lett. **84**, 4502 (2004).
[15] N. R. Madsen, E. G. Gamaly, A. V. Rode, and B. Luther-Davies, J. Phys.: Conf. Ser. **59**, 762 (2007).
[16] M. D. Perry, B. C. Stuart, P. S. Banks, M. D. Feit, V. Yanovsky, and A. M. Rubenchik, J. Appl. Phys. **85**, 6803 (1999).
[17] E. G. Gamaly, A. V. Rode, and B. Luther-Davies, J. Appl. Phys. **85**, 4213 (1999).
[18] A. V. Rode, B. Luther-Davies, and E. G. Gamaly, J. Appl. Phys. **85**, 4222 (1999).
[19] E. G. Gamaly, A. V. Rode, B. Luther-Davies, and V. T. Tikhonchuk, Phys. Plasmas **9**, 949 (2002).
[20] E. G. Gamaly, A. V. Rode, O. Uteza, V. Kolev, B. Luther-Davies, T. Bauer, J. Koch, F. Korte, and B. N. Chichkov, J. Appl. Phys. **95**, 2250 (2004).
[21] S. Amoruso, G. Ausanio, M. Vitiello, and X. Wang, Appl. Phys. A: Mater. Sci. Process. **81**, 981 (2005).
[22] E. M. Lifshitz and L. P. Pitaevskii, *Physical Kinetics* (Pergamon Press, Oxford, 1981).
[23] N. R. Madsen, A. V. Rode, E. G. Gamaly, and B. Luther-Davies, Proc. SPIE **6261**, 62610M (2006).
[24] Ya. B. Zel'dovich and Yu. P. Raizer, *Physics of Shock Waves and High-Temperature Hydrodynamic Phenomena* (Dover, New York, 2002).
[25] M. Mlejnek, E. M. Wright, and J. V. Moloney, Phys. Rev. E **58**, 4903 (1998).
[26] B. Luther-Davies, V. Z. Kolev, M. J. Lederer, N. R. Madsen, A. V. Rode, J. Giesekus, K.-M. Du, and M. Duering, Appl. Phys. A: Mater. Sci. Process. **79**, 1051 (2004).
[27] V. Z. Kolev, M. J. Lederer, B. Luther-Davies, and A. V. Rode, Opt. Lett. **28**, 1275 (2003).
[28] A. V. Rode, D. Freeman, K. G. H. Baldwin, A. Wain, O. Uteza, and Ph. Delaporte, Appl. Phys. A: Mater. Sci. Process. **93**, 135 (2008).
[29] E. G. Gamaly, N. R. Madsen, M. Duering, A. V. Rode, V. Z. Kolev, and B. Luther-Davies, Phys. Rev. B **71**, 174405 (2005).
[30] N. M. Bulgakova, V. P. Zhukov, A. Y. Vorobyev, and C. Guo, Appl. Phys. A: Mater. Sci. Process. **92**, 883 (2008).
[31] A. V. Rode, N. R. Madsen, A. G. Christy, J. Hermann, E. G. Gamaly, and B. Luther-Davies, in *Electronic Properties of Novel Nanostructures*, edited by H. Kuzmany, J. Fink, M. Mehring, and S. Roth, AIP Conf. Proc. No. 786 (AIP, New York, 2005), pp. 96–99.
[32] A. V. Rode, E. G. Gamaly, and B. Luther-Davies, Appl. Phys. A: Mater. Sci. Process. **70**, 135 (2000).
[33] A. V. Rode, R. G. Elliman, E. G. Gamaly, A. I. Veinger, A. G. Christy, S. T. Hyde, and B. Luther-Davies, Appl. Surf. Sci. **197-198**, 644 (2002).
[34] C. Kittel, *Introduction to Solid State Physics* (Wiley, New York, 1996).
[35] http://www.webelements.com/; last visited 7 April 2009.
[36] T. A. Witten, Jr. and L. M. Sander, Phys. Rev. Lett. **47**, 1400 (1981).
[37] S. Amoruso, G. Ausanio, R. Bruzzese, M. Vitiello, and X. Wang, Phys. Rev. B **71**, 033406 (2005).
[38] N. Jegenyes, J. Etchepare, B. Reynier, D. Scuderi, A. Dos-Santos, and Z. Tóth, Appl. Phys. A: Mater. Sci. Process. **91**, 385 (2008).
[39] A. V. Rode, E. G. Gamaly, A. G. Christy, J. D. Fitz Gerald, S. T. Hyde, R. G. Elliman, B. Luther-Davies, A. I. Veinger, J. Androulakis, and J. Giapintzakis, Phys. Rev. B **70**, 054407 (2004).
[40] D. Arčon, Z. Jagličič, A. Zorko, A. V. Rode, A. G. Christy, N. R. Madsen, E. G. Gamaly, and B. Luther-Davies, Phys. Rev. B **74**, 014438 (2006).